Plasma Medicine, 7(1):7–26 (2017)

Real-Time Monitoring of Intracellular Chemical Changes in Response to Plasma Irradiation

Aniruddha Ray,[a] Pietro Ranieri,[b] Leshern Karamchand,[a] Benjamin Yee,[b] John Foster,[b,*] & Raoul Kopelman[a,*]

[a]Department of Chemistry and Biophysics, University of Michigan, Ann Arbor, MI; [b]Department of Nuclear Engineering and Radiological Science, University of Michigan, Ann Arbor, MI

*Address all correspondence to: John Foster, Department of Nuclear Engineering and Radiological Science, 2355 Bonisteel Boulevard, University of Michigan, Ann Arbor, MI, E-mail: jefoster@umich.edu; or Raoul Kopelman, Department of Chemistry and Biophysics, 930 N. University Avenue., University of Michigan, Ann Arbor, MI, E-mail: kopelman@umich.edu

ABSTRACT: Atmospheric pressure nonthermal plasma has shown great potential for medicine applications related to disease treatment. However, the microscopic interaction of the plasma particles and its associated fields with mammalian cells is still not well understood. Here, we present the first *in situ* observation of the fundamental processes related to the chemical changes inside live cells upon plasma irradiation, in real time. We analyze the effect of plasma dose on cell viability and on the internal chemical environment, using novel nano and molecular chemical sensors, in gliosarcoma cells. A pulsed nanosecond helium plasma jet was used as the plasma source. Our results show the accumulation of oxidative and nitrosative stress following two minutes of plasma irradiation, with the initiation of cell death only after three minutes of plasma irradiation. Moreover, the cell membrane integrity became compromised following six minutes of irradiation, which led to sudden changes in the intracellular chemical composition. We also present the first study involving the effects of plasma irradiation on lysosomes and the mitochondrial reduction potential. We observe that the intracellular accumulation of the ROS and RNS has negligible effects on the endosomal and lysosomal membrane integrity, suggesting that the cell membrane damage is likely caused by the external ROS and not by buildup of internal oxidative stress due to the irradiation. These observations illustrate the utility of nanoprobes and molecular probes in providing insight into the fundamental interaction of cold plasma with cells, thereby assisting in the interpretation of observed macroscopic effects of tissue exposed to plasma.

KEY WORDS: plasma medicine, oxidative stress, nitrosative stress, pH, chemical sensing, nanosensors, mammalian cells, fluorescence confocal microscopy

I. INTRODUCTION

Understanding the effects of plasma irradiation on living tissue has garnered a great deal of interest in recent years.[1–7] This interest in plasma irradiation of living tissue is motivated by the resulting positive physiological changes observed in otherwise diseased tissue after plasma treatment.[1,8–10] Currently, the use of plasmas for healthcare is being developed, with applications including wound healing, dental procedures, sterilization, and cancer therapy.[1,3,6,11–13] The majority of these studies focus on essentially macroscopic changes in tissue, during and after irradiation. Currently lacking is a detailed understand-

1947-5764/17/$35.00

ing of the instantaneous internal chemical changes induced in the cells upon plasma irradiation. That is, we do not yet understand how plasma exposure affects the intrinsic cellular and metabolic processes of individual cells in real time.[3,14] Such an understanding would reveal the mechanisms behind the observed curative effects of plasma irradiation and allow us to develop standard plasma dosage regimens for various clinical applications. This insight would also help to better understand how cells respond to plasma exposure, thereby elucidating curative effects and quantifying regimes of cytotoxicity.

In addition, there is an absence of diagnostics with the capacity to monitor plasma-induced chemical changes within individual cells. Rather, the state of the art approach is to characterize the ionized gas phase or the media in which the cells grow. The viability of the cells under such exposure is then assessed. Such a macro approach does not directly address the plasma-induced physical and chemical processes occurring within individual cells in real time.[9,15] Indeed, it can be argued that only with a detailed understanding of plasma-induced mechanisms within the cell itself can treatment plans for sterilization or wound care[16] and other plasma therapy be credibly developed.[12] In this work we address this need.

Conventionally, internal cell physiology can be monitored in a variety of ways. These include physical microprobes and methods such as magnetic resonance and optical imaging. Physical microprobes, the most commonly used approach; often involve the use of microelectrodes and sensing elements that are manually inserted directly into the cell. However, these probes are highly invasive in nature and cannot be used for high resolution mapping of intracellular analytes. Optical probes are attractive because they are highly sensitive, noninvasive, and able of faithfully monitoring dynamic changes inside the cells. Optical probes are generally luminescence based molecular probes or nanoprobes that are assimilated by the cell, either passively via diffusion across the cell membrane, or actively via the cell's endocytic machinery. The changes in fluorescence intensity, or in its upper-state lifetime, are used to monitor the changes in intracellular analyte concentration.[16–18] The probes have been developed, with varying degrees of selectivity, in which specific subcellular elements inside the cytoplasm as well as in the membrane can be monitored.

Here we present the first real-time *in situ* observation of the intracellular chemical changes in response to plasma irradiation, using fluorescence microscopy and novel probes, both nano and molecular. Specifically, we measure the instantaneous changes in intracellular acidity (pH), reactive oxygen species (ROS), and reactive nitrogen species (RNS) in response to plasma irradiation. Intracellular pH changes are of interest as they play a critical role in many cellular events, such as protein synthesis, RNA and DNA synthesis, ion channel conductivity, ion transport, cell cycle control, cellular proliferation, cell fertilization, cell-volume regulation, neurotransmitter reuptake, muscle contraction, and apoptosis.[19] The pH level within microbes, such as bacteria, controls various reaction rates within the cell, as well as the regulation of cell stability and protein structure.[20] In this respect, plasma-induced variations in the cytoplasmic pH are of interest from a sterilization standpoint as well. ROS are produced in copious amounts

in atmospheric pressure plasma discharges, including the aggressive hydroxyl radical (•OH), which can damage lipid molecules and amino acids via bond breakage.[1,2] The migration of this radical, in particular, from the plasma discharge into the cell, is therefore of great interest. An increase in the ROS concentration in cells induces an intracellular oxidative stress that can severely damage the proteins, lipids, and DNA; modulate the cell signaling; and eventually lead to cell death.[21,22] We present a dose-dependent change in the intracellular chemical levels, as well as the viability of cells. We observe the onset of cell death after 3 min of irradiation, and the cells become necrotic following 6 min of irradiation. The increase in the oxidative stress in cells also leads to dysfunction of the cellular organelles, such as lysosomes and mitochondria, which may be a potential cause of cell death. Thus we also indirectly monitor the damage to subcellular components, such as mitochondria, endosomes, and lysosomes, by measuring the dynamic changes in pH and in singlet oxygen levels. This is the first study monitoring such changes to subcellular organelles in response to plasma irradiation. A better understanding of the fundamental processes related to the morphological and chemical changes inside the cells, upon plasma irradiation and in real time, will provide an insights into plasma interactions with live cells and tissues and help optimize plasma therapy. These results should also facilitate its application in clinics.

II. EXPERIMENTAL SETUP

A. Plasma Source

In this study, a nonthermal, atmospheric pressure plasma source was used as the ionized, excited gas source to study plasma cell interactions. Such plasmas are used in plasma medicine studies, because the gas temperature is typically near room temperature, which prevents thermal damage to the cells. Furthermore, such discharges are produced in regular room air, which prevents the dehydration effects associated with the vacuum of conventionally produced plasmas.[23,24] Such plasmas are also used for treatment of polymers and the purification of water.[25] For medical applications, these plasmas, typically produced in helium-oxygen admixtures, produce a host of gas phase products, in particular ROS.[2] It has been shown that the interaction of these ROS radicals, electrons, ions, and UV light, all of which are produced in the plasma discharge, with cells, chemically activate the intracellular medium. This chemically reactive medium is assumed to affect the intracellular environment, which can have positive effects for short exposure times but lead to various forms of cell death for longer exposures.[26] In this work, a helium-fed plasma jet was used. The flow rate was low enough to prevent detachment of cells from their substrate, but still high enough to offset turbulence effects generated downstream. The plasma jet is produced using a coaxial electrode geometry, with a single, metal ground electrode downstream of the powered electrode, depicted schematically in Fig. 1. A pulsed power source applies a 150 nsec rise time, 10 nsec width, and 8 kV amplitude voltage pulse, at a repetition rate of 1 kHz to produce the jet. The voltage pulse creates an ionization wave that travels along the exhaust gas, producing radicals along

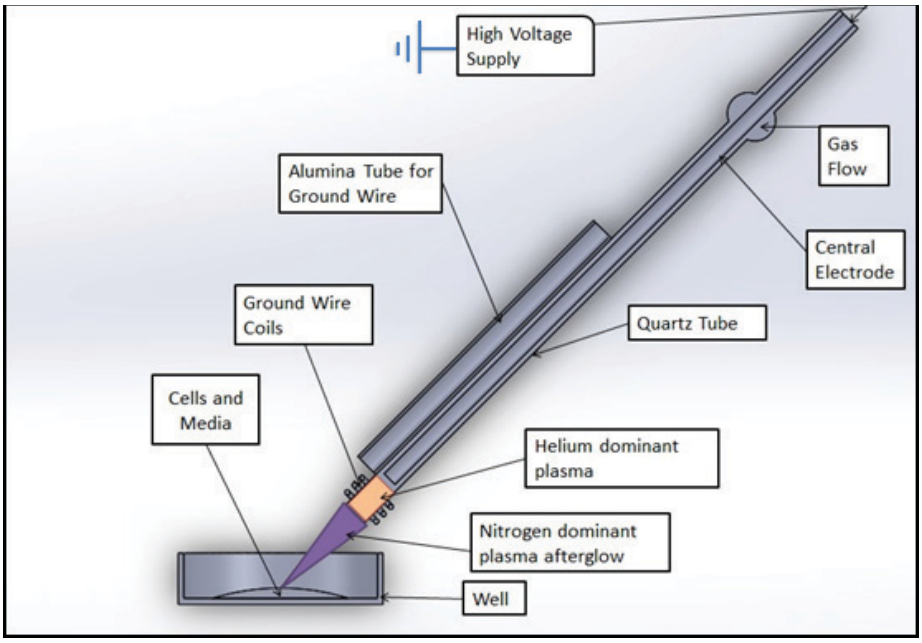

FIG. 1: Schematic depiction of plasma jet processing cells in culture

its length. Details of the mechanics of similar jets, particularly those used for plasma medicine studies, have been published.[25]

B. Cell Culture

The 9L rat gliosarcoma cell line was used to evaluate the effects of plasma on cell viability and oxidative stress. The cells were cultured in 10% serum-supplemented RPMI-1640 cell medium. For microscopy assays the cells were plated in a petri dish with cover glass bottom (Nunc Lab-Tek). During the direct plasma irradiation of cells, 2 mL of colorless cell media was used.

C. Cell Viability Assay

A suspension of 9L cells, prepared in 10% serum-supplemented RPMI-1640 cell medium, was seeded into the wells of a Corning 96-well micro plate, at approximately 10,000 cells per well. Twenty-four hours later, the individual wells of the plate were subjected to plasma irradiation, for varying periods at room temperature. Following treatment, 100 mL of WST-8 dye (CCK-8, Dojindo Molecular Technologies, Inc.) was added to each well, containing either control (nonirradiated cells) or plasma-irradiated cells, and incubated for 4 hr. The absorbance was recorded using a Biochrom Anthos 2010 microplate absorbance reader.

The live/dead cell fluorescence assays were performed according to established protocol. Propidium iodide (PI) (2.5 μM) and calcein AM (3 μM) were added to the cells prior to plasma irradiation. Calcein AM easily passes though the membrane and is retained inside the live cells; whereas PI is membrane impermeable and stains the nucleus of necrotic cells. The calcein fluorescence at 530nm (excitation wavelength: 480 nm) and PI fluorescence at 620 nm (excitation wavelength 530 nm) is monitored using fluorescence microscopy to determine the number of live cells and dead necrotic cells.

D. Fluorescence Microscopy

The live/dead cell assay and the changes in the chemical concentration were monitored using a fluorescence confocal microscope (Leica SP-5X). This state-of-the-art microscope has several excitation sources, including a diode laser (405nm), Ar laser (455nm), a supercontinuum source (490–650 nm), and a Ti:sapphire laser (700–950nm). The fluorescence signal is detected using several photomultiplier tubes (PMTs). An acousto-optic tunable filter allows the selection of the emission wavelength range. Using this microscope it is possible to image four channels simultaneously. All the experiments were performed by placing the petri dish containing cells on the objective (mostly ×60 magnification) followed by plasma irradiation.

The cells were kept in the incubator until right before the measurements were taken, with the sample at room temperature and ambient atmosphere. The petri dishes containing the cells were placed on the microscope objective and the "pre-exposure" images were captured. The cells were then exposed to plasma irradiation in the same general location. The measurements before and after irradiation were performed in the same area; thus the same cells were interrogated. Fluorescence images were acquired before the plasma irradiation as well as after the plasma irradiation at specific time intervals. The cells were not exposed to ambient atmosphere for more than 10 min (experimental duration). All measurements were performed in triplicate.

E. Intracellular pH Measurement

Intracellular pH was measured using a pH sensitive dye, seminaphtharhodafluor (5-[and-6]-carboxy SNARF-1, acetoxymethyl ester) (Invitrogen). The cells were incubated in a 15 μM dye solution, for 30 min, and then washed thoroughly before adding colorless RPMI culture medium. The dye has an absorption maximum at 514 nm, and fluorescence emissions at 580 nm and 640 nm were used for determining the pH level using standard procedures.[27] A fluorescence confocal microscope was used to image the cells. The cells were exposed to the helium plasma jet for up to 6 min, after which the cells were immediately imaged at the same spot. The treatment and imaging were performed at the same location on the cell culture dish so that cumulative effects could be assessed. The pH of the endosomes and lysosomes were measured using 8-hydroxypyrene-1,3,6-trisulfonic acid, trisodium salt (HPTS)-based nanoparticle sensors. These

nanosensors have a pH dependent fluorescence response when irradiated at different wavelengths. At lower pH we observe higher fluorescence at 510 nm, when excited at 405 nm, as compared to 455 nm excitation. Whereas at higher pH the fluorescence signal at 510 nm is higher when excited at 455 nm. The ratio between the fluorescence when excited at 405 and 455 nm is used to quantify pH.[18]

F. Measurement of Oxidative Stress

The cells used in this experiment were incubated in a 4.6 μM solution of 2′,7′-dichlorodihydrofluorescein diacetate (H_2DCFDA or DCF) (Sigma-Aldrich) in colorless RPMI medium for 30 min to promote dye uptake. The cells were then washed thoroughly, followed by addition of colorless RPMI. The sensor dye was excited at 488 nm, and the fluorescence emission at 520 nm was used to monitor the oxidative stress in the cells, following plasma irradiation, using previously established protocols.[27,28] A fluorescence confocal microscope was used for this purpose.

The infusion of the ROS, namely singlet oxygen, in the endosomes and lysosomes was determined by using singlet oxygen sensor green (SOSG) based nanoparticle sensor. These nanosensors have a very weak fluorescence signal; however, in the presence of singlet oxygen we observe a drastic increase in the fluorescence emission at 525 nm. This increase in fluorescence emission is directly proportional to the concentration of singlet oxygen in the microenvironment.[29]

G. Synthesis of Nanosensors

1. Materials

Acrylamide, methylene-bis-acrylamide (MBA), dioctyl sulfosuccinate, Brij 30, hexane, ammonium persulfate (APS), and *N*,*N*,*N*′,*N*′-tetramethylethylenediamine (TEMED), were all acquired from Sigma-Aldrich (St. Louis, MO). *N*-(3-aminopropyl)methacrylamide hydrochloride salt (APMA) was obtained from Polysciences Inc. (Warrington, PA). Ethanol (95%) was acquired from Decon Labs, Inc. (King of Prussia, PA). All solutions were prepared in 18 MΩ water purified in a Barnstead 1 Thermolyne Nanopure II system. All the chemicals and materials were used as received. SOSG and HPTS were obtained from Invitrogen.

2. Methods

The polyacrylamide nanoparticles were synthesized using the process of reverse micelle polymerization technique.[16,18] This technique involves formation of water nano droplets, containing the monomers, stabilized by surfactants in an oily hexane solution. First, the monomer solution was prepared by dissolving 8.6 mmol acrylamide, 0.25 mmol APMA, and 1.2 mmol of the cross-linker in 1.6 mL phosphate buffer at pH 7.4. The choice of cross-linker is mainly governed by the hydrophilicity of the molecule be-

ing incorporated. The pH sensors were prepared using the cross-linker MBA, whereas the singlet oxygen sensors were prepared using GDMA, which is relatively more hydrophobic. The oil solution was prepared by mixing two surfactants, 6.85 mmol Brij 30 and 2.88 mmol dioctyl sulfosuccinate, into 36 mL of the argon-purged hexane solution. The aqueous solution is then added to the hexane solution and stirred for half an hour under inert atmosphere, to stabilize the droplets. The polymerization reaction is initiated by adding 0.54 mmol TEMED and 28 μmol APS, freshly prepared 10% (weight/volume). The solution was further stirred for 2 hr to complete the polymerization. Hexane was removed by rotary evaporation, using a Rotavapor-R (Brinkmann Instruments), and then suspended in ethanol. The surfactants and excess dye were removed by washing the particles five times in ethanol and five times in water for over two days, in an Amicon ultrafiltration cell (Millipore Corp., Bedford, MA), using a 300 kDa filter, and then freeze-dried with a 5 L Modulyo freeze dryer. The molecular dyes can be incorporated into the nanoparticle by encapsulation before the synthesis, or after the nanoparticle synthesis by post loading. The pH sensors were prepared by encapsulating the dye HPTS into the nanoparticle matrix. Whereas the singlet oxygen sensors were prepared by post loading the dye SOSG (singlet oxygen sensor green) into the hydrophobic nanoparticle matrix.

H. Particle Size and Charge

The particles were diluted in water at a concentration of 1 mg/mL, and the particle size distribution in the aqueous solution was measured by dynamic light scattering (DLS) using a DelsaNano C Submicron Particle Size Analyzer (Beckman-Coulter, Brea, CA). The surface charge was measured using the same instrument by monitoring the mobility of the nanoparticles.

I. Nanoparticle-Aided Intracellular Measurements

The 9L cells were plated on a petri dish with a cover glass bottom and grown for a few days before incubation with NPs. The nanosensors were incubated with the cells at 1 mg-mL^{-1} final concentration for 6 hr. After each incubation, unbound nanoparticles (NPs) were removed by gentle rinsing with fresh cell media three times. For the colocalization assay the cells were treated with a lysosomal staining probe, LysoTracker red DNB-99, for 10 min. The excess LysoTracker probe was removed by washing with colorless RPMI media one more time. The colocalization percent is obtained using an ImageJ colocalization plugin.

J. Statistical Analysis

The statistical analyses were performed using one-way analysis of variance (ANOVA) test and were followed up with the Tukey test, which compares every mean with each other and reports the *P* value for each comparison. These analyses were performed using

GraphPad Prism software. All analyses were performed with a confidence interval set at 95% ($P < 0.05$). All the experiments were performed in quintuplicate.

III. RESULTS AND DISCUSSION

The hydrodynamic size of the nanosensors is about 70 nm. They also have a positive surface charge varying from +10 mV to +20 mV. The small size and positive charge facilitates excellent uptake of the nanoparticles by the cells. These nanoparticles also do not show any toxicity by themselves, as shown in Fig. S1, and this is also consistent with our previously published results. The choice of cross-linker for the nanoparticles is important and is based on the molecular dye to be encapsulated, as this controls the degree of hydrophilicity of the nanoparticle. Dyes that are hydrophobic cannot be easily loaded into a hydrophilic matrix. Thus, for SOSG, which is a hydrophobic molecule, we use a slightly modified nanoparticle with GDMA (glycerol dimethacrylate) as the cross-linker instead of MBA. The presence of GDMA makes the matrix hydrophobic, thus facilitating efficient loading of SOSG. However, for HPTS, which is a hydrophilic dye, we used MBA as the cross-linker.

A. Cell Viability and Mitochondrial Reduction Potential

We first investigated the cell viability, using a colorimetric cell viability assay, which is based on the reduction of a water-soluble tetrazolium dye, by cellular dehydrogenases, to its formazan derivative. The tetrazolium dyes are reduced in the mitochondria, and this procedure gives a direct estimation of the mitochondrial reduction potential. Tetrazolium dyes are characterized by a central, positively charged, quaternary tetrazole ring core containing four nitrogen atoms. Upon reduction, the tetrazole ring is disrupted, resulting in a brightly colored formazan derivative. The amount of tetrazolium dye that is reduced to formazan derivatives is directly proportional to the reducing potential of the cell, and hence its viability.[30] Spectrophotometric measurement of the absorbance of the formazan product, produced in cells treated with plasma, relative to that of control (untreated) cells, facilitates the determination of the cytotoxicity of that agent. The CCK-8 assay used here is a tetrazolium based assay. The reduction of these salts is associated with not only mitochondria, but also the cytoplasm and with nonmitochondrial membranes, including the endosome/lysosome compartment and the plasma membrane. The percentage viabilities of the plasma-irradiated cells are calculated by measuring the absorbance of the formazan derivative at 490 nm, and they are reported relative to the viability of the control cells, as shown in Fig. 2. We observed the onset of cell death from 3 min irradiation onwards. This is a very crucial parameter, towards *in vivo* application, for determining the plasma irradiation dose of such a source, without damaging the host cells. In our case the number of cells irradiated is only a fraction (15%) of the total number of cells because of the larger size of the wells compared to the plasma irradiation diameter. Thus, the cell viability was calculated based on the following formulae

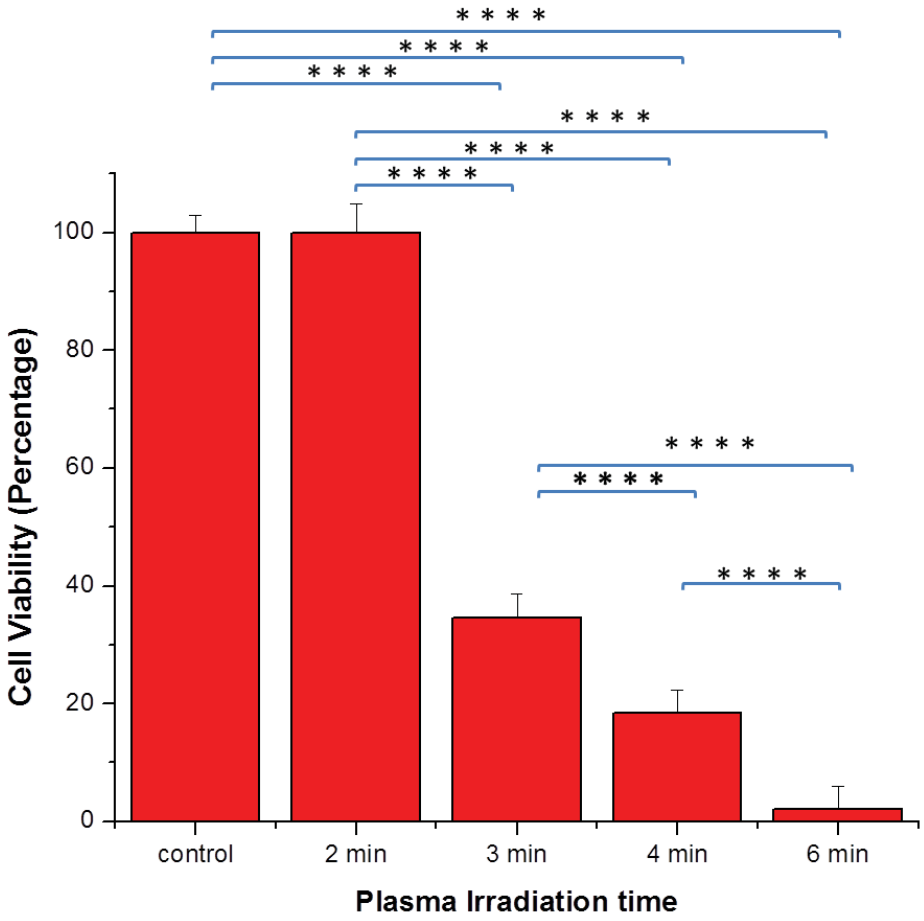

FIG. 2: Cytotoxic effect of plasma irradiation on 9L cells, using CCK-8 assay. Viability of the control cells, without any plasma irradiation, is set to 100%. Error bars show standard deviations. The *P* values are denoted as shown: **P* < 0.05; ***P* < 0.01; ****P* < 0.001; *****P* < 0.0001.

$$\textit{Percent Viability}\ (\textit{Plasma irradiation time} = t) = (I_t - I_\infty) / (I_0 - I_\infty) \quad \text{x} \quad 100$$

I_t: Absorbance of formazan dye for samples with plasma irradiation time '*t*'
I_∞: Absorbance of formazan dye for samples with plasma irradiation for sufficiently long time to kill all cells in the exposure area (obtained from microscopy data)
I_0: Absorbance of formazan dye for samples without plasma irradiation.

It has been previously shown that plasma irradiation can cause mitochondrial depolarization, leading to apoptosis.[31] Our results corroborate the previous findings.

In addition to the CCK-8 assay, the cell morphology and the onset of necrosis were also monitored, using calcein AM and propidium iodide tests. Cell death can occur

through apoptosis or necrosis. Apoptosis is programmed cell death, whereas necrosis occurs when the integrity of the cell membrane is compromised. Necrosis, *in vivo,* can lead to uncontrolled inflammatory responses and other undesirable effects. The onset of necrosis can be monitored by using PI, which is a membrane impermeable dye that only stains the nucleus of necrotic cells. The cells before plasma treatment do not show any PI staining but have excellent calcein staining, as shown in Fig. S2. From the CCK-8 data, we observe cell death after 3 min irradiation, but we do not observe any PI staining, even after a few hours, indicating that the most likely cause of cell death is apoptosis. These results corroborate previous reports on the observation that extended exposure to nonthermal plasma leads to apoptosis.[32,33] It has been shown that plasma exposure results in the activation of p53 in certain cell lines, which delays the cell cycle process and leads to apoptosis. It is claimed that this method will be particularly useful for cell lines resistant to chemotherapy.[32] Another study showed that irradiating cells with plasma activate c-Jun NH_2-terminal kinase (JNK) and p38 kinase, due to the presence of ROS and RNS, that leads to apoptosis.[33] We observed an instantaneous change in the cellular morphology, following 4 min of plasma irradiation. A majority of the cells start to bleb, which is pinching of the cell membrane, although we do not observe any instantaneous PI staining. On further increasing the irradiation time to 5 or 6 min, we observed immediate nuclear staining from PI, which is indicative of necrosis. Figure 3 shows the cellular morphology and the staining, following 4 and 6 min of plasma irradiation. We observed a strong calcein fluorescence and no signal from PI after 4 min irradiation. However, we did observe significant cell blebbing, indicating apoptosis. For the 6-min irradiation period, we observed a weak calcein fluorescence and a strong PI signal indicating necrosis. The weak calcein fluorescence is attributed to the leakage of dye from the cytosol because the cell membrane is heavily compromised. Thus, combining the results from the previous CCK-8 assay and the calcein-PI assay, we can evaluate the type of cell death following different plasma doses.

B. Cytosolic Chemical Changes

1. Oxidative Stress in Cells

Next, we investigated the oxidative stress in the 9L cells. It has been previously shown that the plasma jets produce ROS, such as singlet oxygen, peroxides, nitrites, and hydroxyl radicals. The probe DCF is a membrane permeable dye that is initially nonfluorescent.[17,34] However, the probe becomes highly fluorescent following cleavage of its two acetate groups by intracellular esterase enzymes, and oxidation following interaction with the ROS species. We irradiated the cells for several time periods, up to 6 min, as shown in Fig. 4a. We observed the development of oxidative stress after only *1 min* of plasma irradiation, although it becomes quite significant after only 2 min. This may be the onset of lipid peroxidation, although we do not observe any significant increase in toxicity until after 3 min of irradiation, as shown in Fig. 2. However, after 6 min of

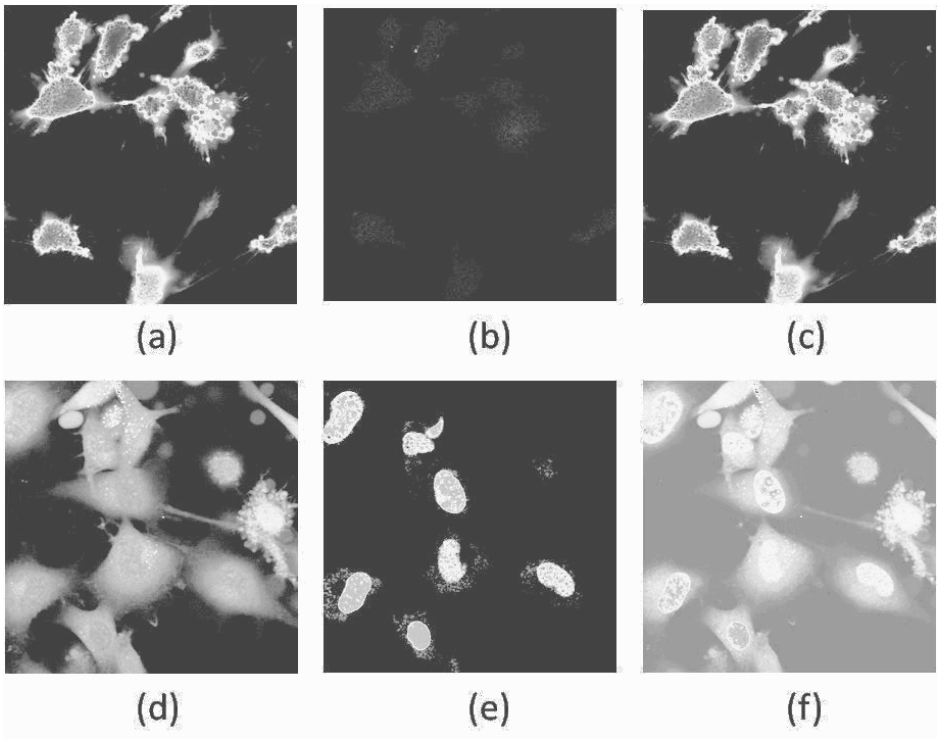

FIG. 3: Cells stained with calcein and PI, following 4 min (top) and 6 min (bottom) irradiation. Cells stained with calcein (a and d) and PI (b and e). The overlay of the green and red is shown in parts c and f. For the 4-min irradiation, we do not observe any damage to the membrane integrity and hence no red fluorescence from the nucleus (b). However, for the 6-min treatment, we see significant nuclear staining, which is indicative of instantaneous necrosis (e).

irradiation, a further increase in the ROS concentration was observed. This is consistent with our observation of the pH changes elicited following plasma exposure, and may be attributed to the damaged cell membrane and malfunctioning ion channels. Similar increase in the ROS level in cells was also reported previously, although after a much longer time duration.[33] They observed a threefold increase in intracellular ROS level after 1 hr post irradiation, but the oxidative stress reduced with time. However as shown in Fig. 4b, we observe more than a 100-fold increase in the level of ROS in the extracellular environment (cell media).

2. Nitrosative Stress in Cells

Reactive nitrogen species (RNS) are a set of molecules and free radicals, including nitric oxide and its derivatives, such as nitrogen dioxide radical, peroxynitrite anion, peroxynitrous acid, nitrosoperoxycarbonate anion, nitronium cation, and dinitrogen trioxide.[35] In addition to the ROS, a cold plasma also produces significant amounts of

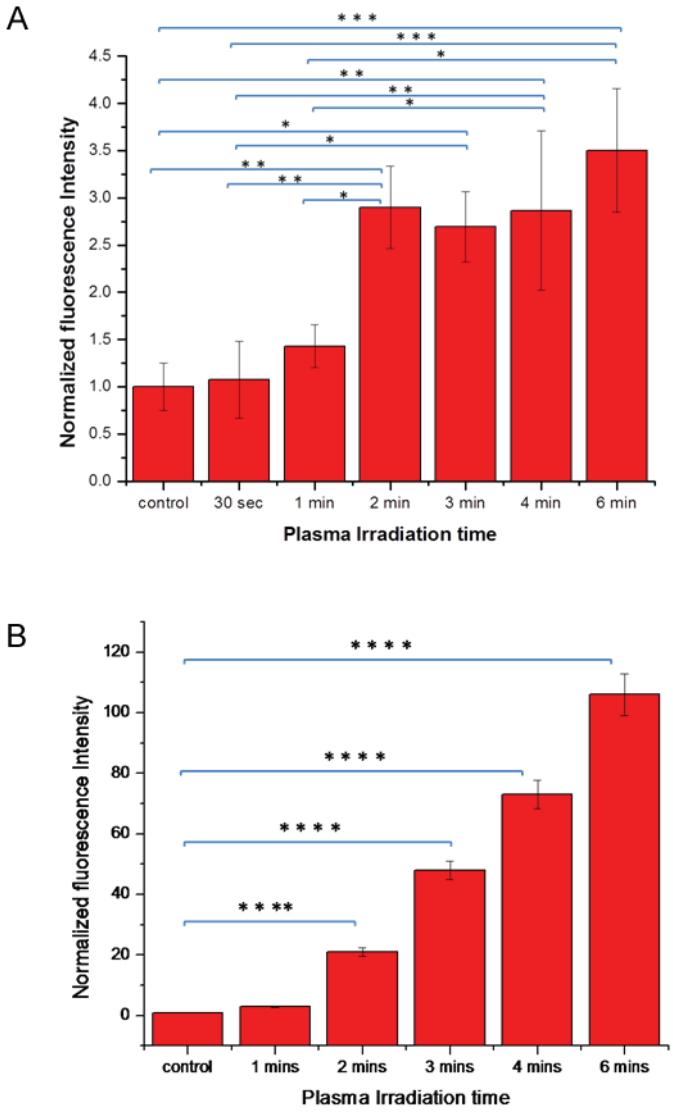

FIG. 4: (a) Fluorescence emission intensity of DCF dye at 520 nm inside the 9L cells, following plasma irradiation, showing oxidative stress. (b) Fluorescence intensity from DCF dye in the extracellular environment indicating the changes in the level of ROS in cell media. Error bars show standard deviations. The *P* values are denoted as shown: *$P < 0.05$; **$P < 0.01$; ***$P < 0.001$; ****$P < 0.0001$.

RNS. Like the ROS, the RNS play a critical role in many biological functions, such as signal transduction, cellular signaling, regulation of cell growth, and neurotransmission. However, an imbalance in the amount of RNS can lead to stress in the cells. They interact and oxidize the subcellular components and membrane, which eventually leads

to cell death.[35] We determined the increase in intracellular RNS using a dye, DAF-FM (4-amino-5-methylamino-2′,7′-difluorofluorescein). DAF-FM diacetate is a cell permeable dye; it easily penetrates the cell membrane and is then cleaved by intracellular esterases and retained inside the cytoplasm.[17] Once the DAF dye is oxidized, it then interacts with NO to form a fluorescent triazole compound, leading to an increase in its fluorescence quantum yield of almost two orders of magnitude. This increase in fluorescence is used to monitor the qualitative changes in the amount of intracellular NO. Figure 5 shows the changes in the intracellular RNS. We observe a significant increase in the amount of RNS, from 2 min of irradiation onwards, constantly increasing with longer irradiation times, until 4 min. The amount of RNS increases drastically after 6 min, because of cell membrane damage. These results are in accordance with our previous observations with ROS. Previous long term studies on the evolution of the intracellular RNS showed a slight increase (2×) in the concentration level from 1 hr up to 18 hr, and then decreased within 48 hr.[33] We also observe an increase in the RNS levels by a factor of 30 in the extracellular environment, as shown in Fig. 4b,which is significantly lower than the observed increase in ROS levels.

Although most of these probes lack absolute specificity towards a particular species, they display high sensitivity towards some of the ROS or RNS, thereby providing a basis for the estimation of their relative contributions to the intracellular effects.[36] These measurements provide a qualitative idea of the temporal evolution of each of the ROS and RNS inside the cytoplasm, in response to plasma exposure.

3. Intracellular pH Measurement

The NO_x and some of the ROS produced from plasma irradiation can reduce the pH level. The plasma driven reduction in pH has been exploited to kill bacteria.[37,38] Thus we monitored the intracellular pH level of the cells to determine if the plasma irradiation gave rise to any reduction in intracellular pH, that might contribute towards the cell death. The pH change was measured after 3 min of irradiation. Additionally, the change in intracellular pH level can also be an indication of the improper functioning of the ion channels, caused by plasma irradiation.

SNARF-1 AM-ester which is a pH sensitive, cell permeant dye, was used to monitor the pH response in the cytoplasm. The dye permeates the cell membrane and accumulates in the cytoplasm following de-esterification by the intracellular esterase enzymes that render the molecule membrane impermeable.[39,17] Figure 6(a) shows the SNARF loaded cells after 6 min of irradiation. We did not observe any significant change in pH for irradiation shorter than 6 min. However, after 6 min of irradiation, we observed a slight increase in pH (up to +0.2 pH units). This may be attributed to the influx of ions from the extracellular culture medium into the cytoplasm, due to compromised membrane integrity. The relative insensitivity of the intracellular pH to plasma exposure was surprising, because air plasma irradiated water solutions have been shown to decrease the pH of the medium.[40] However these results show that the

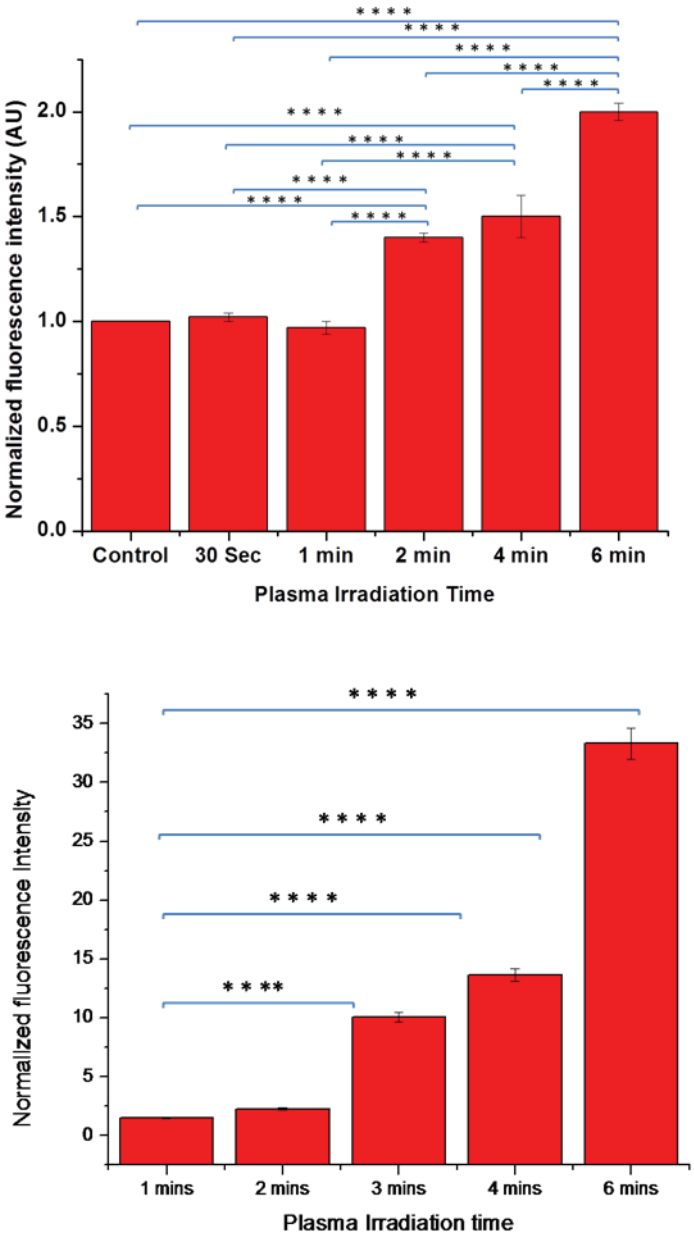

FIG. 5: (a) Fluorescence intensity from DAF inside the cytoplasm, following different plasma irradiation periods, indicating nitrosative stress. (b) Fluorescence intensity from DAF in the extracellular environment indicating the changes in RNS in cell media. Error bars show standard deviations. The *P* values are denoted as shown: **P* < 0.05; ***P* < 0.01; ****P* < 0.001; *****P* < 0.0001.

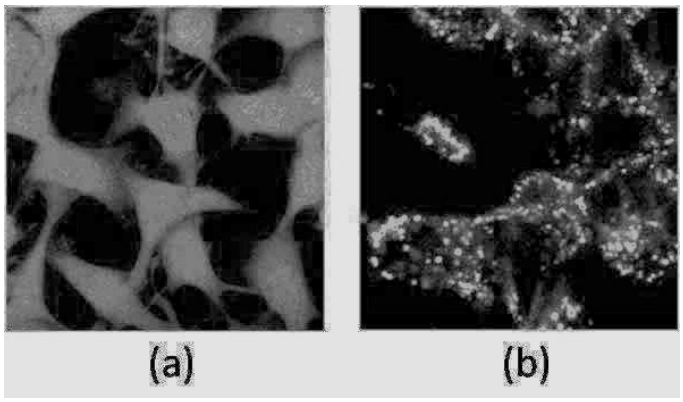

FIG. 6: 9L cells containing the (left) pH sensitive SNARF dye (a), (right) pH sensitive nanoparticles containing HPTS (b). The molecular probes selected for monitoring the pH at different intracellular component is based on their pKa value. The dye, which is membrane permeable, is uniformly spread throughout the cytoplasm, whereas the NPs are localized in compartments. The images were taken in the confocal mode, with a ×40 objective (scale, 20 μm).

cell death cannot be attributed to the internal changes in pH, which is an extremely important physiological factor.

C. Chemical Changes in Endosomes and Lysosomes

Lysosomes are cell organelles responsible for the degradation of proteins and macromolecules that have been endocytosed or phagocytosed. The lysosomes consist of many degradative enzymes. Disrupting the membrane leads to a leakage of such enzymes into the cytoplasm.[41] It has been previously shown that the reactive oxygen and nitrogen species can damage the lysosomes by destabilizing the membrane through lipid peroxidation. This in turn can lead to dysfunction of the cell, and even its death, by inducing apoptosis.[42–44] We observed the perturbation to the lysosome by monitoring the pH changes. It has been previously shown that the pH of lysosomes tends to increase when the membrane integrity is compromised because of oxidative stress. We monitored the changes in lysosomal pH using polyacrylamide-based nanosensors. The nanosensor consists of a pH sensitive fluorescent dye, HPTS, encapsulated in a polyacrylamide matrix. Figure 6 shows the pH sensitive fluorescent nanosensors in the cells. This type of HPTS nanosensors has been previously used for measuring the pH of lysosomes and endosomes.[18,45]

These nanosensors get endocytosed by different pathways, such as those mediated by clathrin and caveolae, and tend to accumulate in the acidic vesicles, such as the lysosomes.[46] To monitor the colocalization of these nanoparticles with the acidic vesicles, we stained the acidic compartments with LysoTracker dye and monitored the overlap between the fluorescence from the nanoparticles and that of the stain. LysoTracker dyes selectively stained the acidic vesicles. Figure 7 shows the overlap of the fluorescence

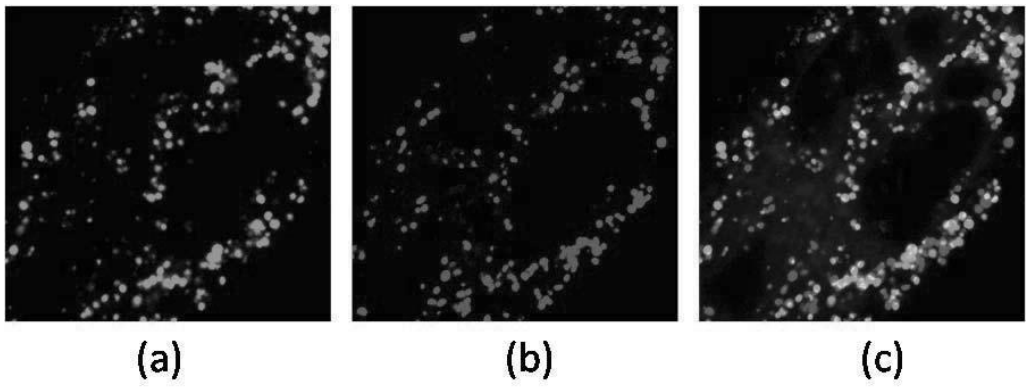

Fig. 7: Co-localization of the nanoparticles with lysosomes. (a) The nanoparticles inside cells (green fluorescence); (b) The staining of the lysosomes using lysotracker dye (red fluorescence). (c) The co-localization of the nanoparticles and lysosomes is shown here (yellow and orange, due to overlap between green and red).

signal from the nanoparticles with that from the LysoTracker. We observed that about 41% of the total number of nanoparticles, internalized by the cells, are localized inside the lysosomes. The rest of the nanoparticles are most likely in late endosomes or other vesicles such as caveosomes. These nanoparticles are completely nontoxic, and we do not observe any oxidative stress due to the nanoparticles, even after 48-hr incubation.[28,18]

Upon plasma irradiation we do not observe any changes in the pH of the local environment of the nanoparticles, for up to 6 min of irradiation. This indicates that, although there is a significant buildup of ROS inside the cytoplasm, they do not disrupt the endosomes and lysosomes.

Additionally, we also monitored the diffusion of the ROS, singlet oxygen in particular, into the endosomes. For this purpose we used nanoparticles loaded with singlet oxygen sensor green (SOSG), which is a membrane impermeant dye that has a very weak fluorescence. However, on interacting with singlet oxygen, its fluorescence increases significantly because of oxidation.[17] The increase in fluorescence can be used to detect the presence of singlet oxygen. SOSG was chosen for this purpose for two reasons: (1) the molecules are membrane impermeant and thus will not leak into the cytoplasm if they leach out of the nanoparticle matrix; and (2) the molecules are extremely sensitive to the presence of singlet oxygen, but not to other ROS and can be used for dynamic monitoring. We did not observe any changes in the fluorescence signal from the nanoparticles until 6 min irradiation. However, on irradiating further, we observed a steady increase of fluorescence signal. This is due to the sudden increase of ROS species in the cytoplasm after 6 min, when most of the cells become necrotic. This increase in ROS probably leads to the peroxidation of the lipid in the vesicles. Thus both the pH and singlet oxygen sensing experiments show that the intracellular vesicles, like the endosomes and lysosomes, are unperturbed by the buildup of ROS in the cytoplasm, until the cells become necrotic.

IV. CONCLUSION

In summary, we have investigated the immediate internal chemical environment of living cells exposed to nonthermal plasma. Here we observed that the plasma conditions investigated did not elicit significant changes in the intracellular pH level. However, we did observe that the plasma interaction with the media produces large amounts of ROS and RNS, and thus we observed the onset of oxidative stress inside cells after just a *1 min* irradiation. The level of oxidative stress not only affects the cell signaling but also has the potential to damage the cell components, and is thus a very important parameter in determining the dose of plasma irradiation. Not surprisingly, the cell viability assays show significant cell death after only 3 min of plasma irradiation. In conclusion, the intracellular chemical probes presented here provide critical insights into the interaction of plasma and mammalian cells, and can serve as a powerful tool for assessing the response of cells to plasma irradiation in future plasma medicine studies. This tool allows for the quantification of plasma-induced effects and, ultimately, quantification of actual plasma therapies.

ACKNOWLEDGMENTS

The authors acknowledge NSF grant: CBET 1249787. The authors would also like to thank Ananya Mukundan for her assistance during the experiments.

REFERENCES

1. Fridman A, Friedman G. Plasma medicine. West Sussex, UK: Wiley; 2013.
2. Graves DB. The emerging role of reactive oxygen and nitrogen species in redox biology and some implications for plasma applications to medicine and biology. J Phys D: Appl Phys. 2012;45:263001–42.
3. Lloyd G, Friedman G, Jafri S, Schultz G, Fridman A, Harding K. Gas plasma: medical uses and developments in wound care. Plasma Process Polym. 2010;7:194–211.
4. Fridman G, Friedman G, Gutsol A, Shekhter AB, Vasilets VN, Fridman A. Applied plasma medicine. Plasma Process Polym. 2008;15: 503–33.
5. Morfill GE, Kong MG, Zimmermann JL. Focus on plasma medicine. New J Phys. 2009;11:115011–8.
6. Laroussi M. Low temperature plasma-based sterilization: overview and state-of-the-art. Plasma Process Polym. 2005;2:391–400.
7. Robert E, Vandamme M, Brullé L, Lerondel S, Le Pape A, Sarron V, Ries D, Darny T, Dozias S, Collet G, Kieda C, Pouvesle JM. Perspectives of endoscopic plasma applications. Clin Plasma Med. 2013;1:8–16.
8. Stalder KR, McMillen DF, Woloszko J. Electrosurgical plasmas. J Phys D: Appl Phys. 2005;38:1728–38.
9. Isbary G, Zimmermann JL, Shimizu T, Li YF, Morfill GE, Thomas HM, Steffes B, Heinlin J, Karrer S, Stolz W. Non-thermal plasma—More than five years of clinical experience. Clin Plasma Med. 2013;1:19–23.
10. Isbary G, Köritzer J, Mitra A, Li Y-F, Shimizu T, Schroeder J, Schlegel J, Morfill GE, Stolz W, Zimmermann JL. Ex vivo human skin experiments for the evaluation of safety of new cold atmospheric plasma devices. Clin Plasma Med. 2013;1:36–44.
11. Nosenko T, Shimizu T, Morfill GE. Designing plasmas for chronic wound disinfection. New J Phys. 2009;11:115013–9.
12. Tipa RS, Kroesen GMW. Plasma-stimulated wound healing. IEEE Trans Plasma Sci. 2011;39:2978–9.

13. Kim JY, Wei Y, Li J, Foy P, Hawkins T, Ballato J, Kim SO. Single-cell-level microplasma cancer therapy. Small. 2011;7:2291–5.
14. Samukawa S, Hori M, Rauf S, Tachibana K, Bruggeman P, Kroesen G, Whitehead JC, Murphy AB, Gutsol AF, Starikovskaia S. The 2012 Plasma Roadmap. J Phys D: Appl Phys. 2012;45:253001–37.
15. Weltmann K-D, Polak M, Masur K, von Woedtke T, Winter J, Reuter S. Plasma processes and plasma sources in medicine. Contrib Plasma Phys. 2012;52:644–54.
16. Ray A, Kopelman R. Hydrogel nanosensors for biophotonic imaging of chemical analytes. Nanomedicine (Lond). 2013;8:1829–38.
17. Haugland RP. The handbook: a guide to fluorescent probes and labeling technologies. Buckley, UK: Invitrogen Corp.; 2005.
18. Ray A, Koo Lee Y-E, Epstein T, Kim G, Kopelman R. Two-photon nano-PEBBLE sensors: subcellular pH measurements. Analyst. 2011;136:3616–22.
19. Kurkdjian A GJ. Intracellular pH: measurement and importance in cell activity. Annu Rev Plant Physiol Plant Mol Biol. 1989;40:271–303.
20. Slonczewski JL, Fujisawa M, Dopson M, Krulwich TA. Cytoplasmic pH measurement and homeostasis in bacteria and archaea. Adv Microb Physiol. 2009;55:1–70.
21. Martindale JL, Holbrook NJ. Cellular response to oxidative stress: signaling for suicide and survival. J Cell Physiol. 2002;192:1–15.
22. Joh HM, Kim SJ, Chung TH, Leem SH. Reactive oxygen species-related plasma effects on the apoptosis of human bladder cancer cells in atmospheric pressure pulsed plasma jets. Appl Phys Lett. 2012;053703–5.
23. Stoffels E, Kieft IE, Sladek REJ, Bedem LJM Van Den, Laan EP Van Der, Steinbuch M. Plasma needle for in vivo medical treatment: recent developments and perspectives. Plasma Sources Sci Technol. 2006;15:S169–80.
24. Laroussi M, Lu X. Room-temperature atmospheric pressure plasma plume for biomedical applications. Appl Phys Lett. 2005;87:113902–3.
25. Wang M, Foster JE, Kushner MJ. Plasma propagation through porous dielectric sheets. IEEE Trans Plasma Sci. 2011;39:2244–5.
26. Kalghatgi S, Kelly CM, Cerchar E, Torabi B, Alekseev O, Fridman A, Azizkhan-Clifford J. Effects of non-thermal plasma on mammalian cells. PLoS One. 2011;6:e16270–11.
27. Wiederschain GY. The Molecular Probes handbook. A guide to fluorescent probes and labeling technologies. Biochemistry (Moscow). 2011;76(11):1276.
28. Ray A, Mukundan A, Xie Z, Karamchand L, Wang X, Kopelman R. Highly stable polymer coated nano-clustered silver plates: a multimodal optical contrast agent for biomedical imaging. Nanotechnology; 2014;25(44):445104–9.
29. Yoon HK, Lou X, Chen YC, Koo Lee YE, Yoon E, Kopelman R. Nanophotosensitizers engineered to generate a tunable mix of reactive oxygen species, for optimizing photodynamic therapy, using a microfluidic device. Chem Mater. 2014;26:1592–600.
30. Berridge MV, Herst PM, Tan AS. Tetrazolium dyes as tools in cell biology: new insights into their cellular reduction. Biotechnol Annu Rev. 2005; 127–52.
31. Ahn HJ, Kim K Il, Kim G, Moon E, Yang SS, Lee JS. Atmospheric-pressure plasma jet induces apoptosis involving mitochondria via generation of free radicals. PLoS One. 2011;6,e28154–7.
32. Ma Y, Ha CS, Hwang SW, Lee HJ, Kim GC, Lee KW, Song, K. Non-thermal atmospheric pressure plasma preferentially induces apoptosis in p53-mutated cancer cells by activating ROS stress-response pathways. PLoS One. 2014;9:e91947–14.
33. Ahn HJ, Kim K Il, Hoan NN, Kim CH, Moon E, Choi KS, Yang SS, Lee JS. Targeting cancer cells with reactive oxygen and nitrogen species generated by atmospheric-pressure air plasma. PLoS One. 2014;9:e86173–13.
34. Gomes A, Fernandes E, Lima JLFC. Fluorescence probes used for detection of reactive oxygen species. J Biochem Biophys Methods. 2005;65(2–3)45–80.

35. Martínez MC, Andriantsitohaina R. Reactive nitrogen species: molecular mechanisms and potential significance in health and disease. Antioxid Redox Signal. 2009;11:669–702.
36. Price M, Kessel D. On the use of fluorescence probes for detecting reactive oxygen and nitrogen species associated with photodynamic therapy. J Biomed Opt. 2010;15(5):051605–3.
37. Ikawa S, Kitano K, Hamaguchi S. Effects of pH on bacterial inactivation in aqueous solutions due to low-temperature atmospheric pressure plasma application. Plasma Process Polym. 2010;7:33–42.
38. Traylor MJ, Pavlovich MJ, Karim S, Hait P, Sakiyama Y, Clark DS, Graves DS. Long-term antibacterial efficacy of air plasma-activated water. J Phys D: Appl Phys. 2011;44:472001–4.
39. Han J, Burgess K. Fluorescent indicators for intracellular pH. Chem Rev. 2010;110:2709–28.
40. Foster JE, Weatherford B, Gillman E, Yee B. Underwater operation of a DBD plasma jet. Plasma Sources Sci Technol. 2010;19(2):025001–9.
41. Boya P, Kroemer G. Lysosomal membrane permeabilization in cell death. Oncogene. 2008;27:6434–51.
42. Johansson AC, Appelqvist H, Nilsson C, Kågedal K, Roberg K, Öllinger K. Regulation of apoptosis-associated lysosomal membrane permeabilization. Apoptosis. 2010;15(5):527–40.
43. Zdolsek JM, Svensson I. Effect of reactive oxygen species on lysosomal membrane integrity. A study on a lysosomal fraction. Virchows Arch B Cell Pathol Incl Mol Pathol. 1993;64:401–6.
44. Denamur S, Tyteca D, Marchand-Brynaert J, Van Bambeke F, Tulkens PM, Courtoy PJ, Mingeot-Leclercq MP. Role of oxidative stress in lysosomal membrane permeabilization and apoptosis induced by gentamicin, an aminoglycoside antibiotic. Free Radic Biol Med. 2011;51:1656–65.
45. Ray A, Lee YEK, Kim G, Kopelman R. Two-photon fluorescence imaging super-enhanced by multi-shell nanophotonic particles, with application to subcellular pH. Small. 2012;8:2213–21.
46. Karamchand L, Kim G, Wang S, Hah HJ, Ray A, Jiddou R, Koo Lee YE, Philbert MA, Kopelman R. Modulation of hydrogel nanoparticle intracellular trafficking by multivalent surface engineering with tumor targeting peptide. Nanoscale. 2013;5:10327–44.

SUPPLEMENT A. NP CELL VIABILITY OF BLANK: TOXICITY FROM BLANK NANOPARTICLES WAS OBSERVED USING THE MTT ASSAY, AS DESCRIBED BEFORE

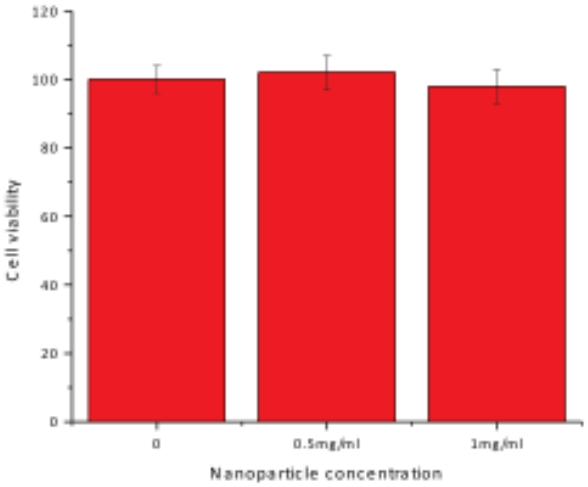

FIG. S1: The toxicity from blank nanoparticles. We did not observe any significant toxicity from the blank nanoparticles, which is consistent with our previously published results.

SUPPLEMENT B. CALCEIN-PI ASSAY ON CELLS BEFORE IRRADIATION

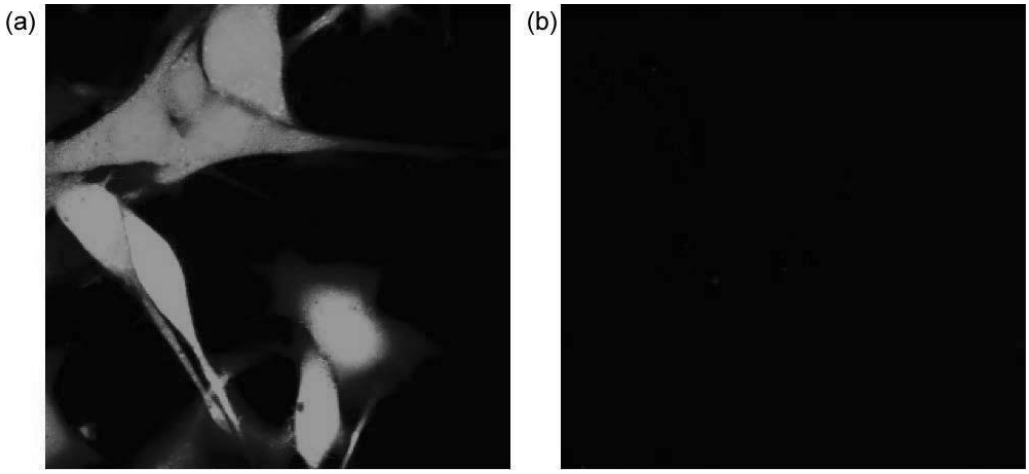

FIG. S2: Cells before plasma irradiation with calcein staining (a) and PI staining (b). We observed strong calcein fluorescence from the cells, indicating that the cells were healthy and there was efficient intracellular accumulation of calcein. We did not observe any PI fluorescence, indicating the absence of necrotic cells.